

Regeneration Profiles of Olfactory Epithelium after SARS-CoV-2 Infection in Golden Syrian Hamsters

Shinji Urata,¹ Junki Maruyama,¹ Megumi Kishimoto-Urata, Rachel A. Sattler, Rebecca Cook, Nantian Lin, Tatsuya Yamasoba, Tomoko Makishima,* and Slobodan Paessler*

Cite This: *ACS Chem. Neurosci.* 2021, 12, 589–595

Read Online

ACCESS |

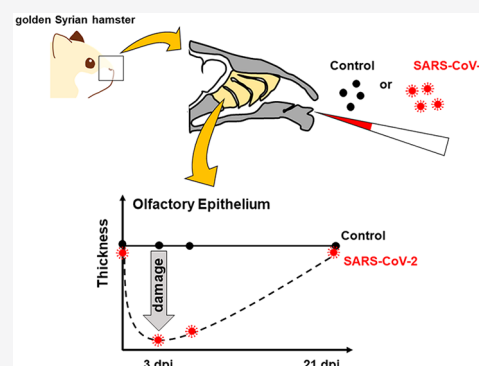
Metrics & More

Article Recommendations

Supporting Information

ABSTRACT: Olfactory dysfunction is one of the most frequent and specific symptoms of coronavirus disease 2019 (COVID-19). Information on the damage and repair of the neuroepithelium and its impact on olfactory function after COVID-19 is still incomplete. While severe acute respiratory syndrome coronavirus-2 (SARS-CoV-2) causes the ongoing worldwide outbreak of COVID-19, little is known about the changes triggered by SARS-CoV-2 in the olfactory epithelium (OE) at the cellular level. Here, we report profiles of the OE after SARS-CoV-2 infection in golden Syrian hamsters, which is a reliable animal model of COVID-19. We observed severe damage in the OE as early as 3 days postinoculation and regionally specific damage and regeneration of the OE within the nasal cavity; the nasal septal region demonstrated the fastest recovery compared to other regions in the nasal turbinates. These findings suggest that anosmia related to SARS-CoV-2 infection may be fully reversible.

KEYWORDS: COVID-19, SARS-CoV-2, olfactory epithelium, olfactory dysfunction, anosmia



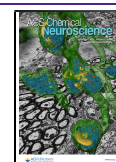
Severe acute respiratory syndrome coronavirus-2 (SARS-CoV-2) is the causative pathogen of coronavirus disease 2019 (COVID-19). Coronaviruses (CoVs) are enveloped, nonsegmented, positive-sense RNA viruses. Human CoVs such as CoV-229E, NL63, HKU1, and OC43 primarily cause mild respiratory diseases, whereas SARS-CoV-1¹ and Middle East respiratory syndrome CoV² may cause severe pneumonia. Similar to these highly pathogenic CoVs, SARS-CoV-2 has been causing acute infection of the lungs in humans since late 2019. While a large proportion of those infected with SARS-CoV-2 are asymptomatic or present only with mild flu-like symptoms, life-threatening pneumonia may develop in severe cases. Anosmia is one specific symptom observed in the majority of patients with confirmed diagnoses across all degrees of severity of SARS-CoV-2 infection.^{3,4} While anosmia occurs primarily in the early stage of COVID-19,^{4,5} it can also manifest at later stages.⁶ Anosmia caused by SARS-CoV-2 is characterized by a sudden onset without any associated nasal symptoms followed by a rapid recovery. Fortunately, patients diagnosed with anosmia by SARS-CoV-2 infection seem to have a better prognosis compared to olfactory dysfunction caused by other viral infections, which is usually permanent.⁷ The olfactory epithelium (OE) consists of three cell types: supporting cells, basal cells, and olfactory sensory neurons (OSNs), which express odorant receptors (ORs). The OE is susceptible to damage through direct exposure to environmental agents entering the nasal cavity. To cope with this continuous injury of the OE, OSNs constantly regenerate

through the proliferation and differentiation of basal cells. Disruption of OE turnover leads to olfactory dysfunction, anosmia, and hyposmia. In addition to olfactory function, the OE serves as a barrier to block infective agents from entering the central nervous system. SARS-CoV-2 binds its specific receptor, human angiotensin converting enzyme II (hACE2), on the surface of target cells for cell entry. hACE2 is expressed not only in type II pneumocytes in the lung³ but also in the supporting cells,⁷ basal stem cells,⁷ perivascular cells,⁷ and goblet secretory cells of the OE,³ suggesting that OE is susceptible to SARS-CoV-2 infection.⁸ The OE is divided into four zones, zones 1 to 4, based on the distribution of specific types of ORs.⁹ Characteristics such as vulnerability and regeneration capability are different in each zone. Generally, the OE in zone 1 is vulnerable to oxidative stress, zones 2–4 have high metabolic rates, and zones 3–4 are vulnerable to viral infections.^{10,11} Characterizing each zone associated with SARS-CoV-2 infection will enable us to understand olfactory dysfunction related to COVID-19. However, profiles of each zone upon SARS-CoV-2 infection have not been characterized in detail. Here, we report detailed histological profiles of the

Received: October 10, 2020

Accepted: January 27, 2021

Published: February 1, 2021



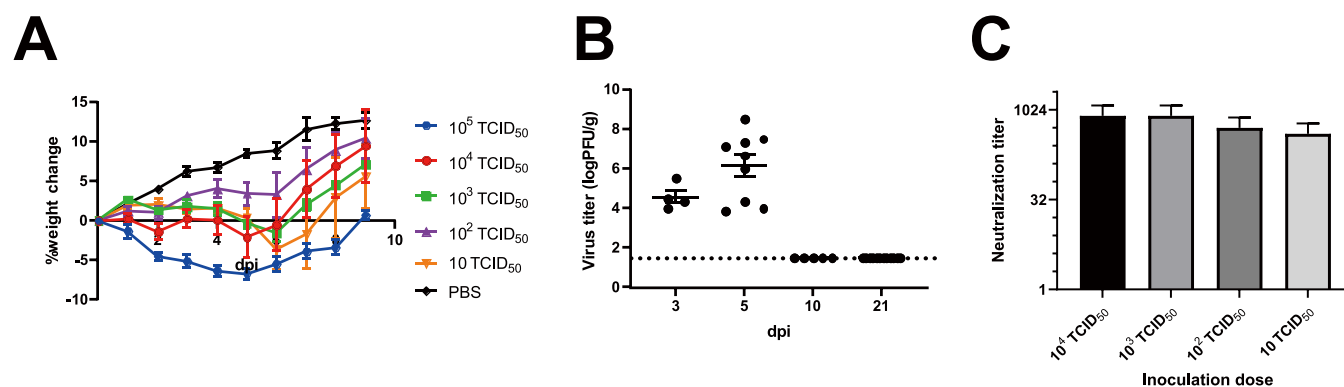


Figure 1. General conditions of golden Syrian hamsters infected with SARS-CoV-2. (A) Averages of percent weight change after infection throughout the study. (B) Virus titers in the lungs of SARS-CoV-2 challenged hamsters (3 dpi, $n = 4$; 5 dpi, $n = 9$; 10 dpi, $n = 5$; 21 dpi, $n = 12$). (C) Neutralizing antibodies in SARS-CoV-2 challenged hamsters on 21 dpi. Average \pm SEM are shown.

four OE zones after SARS-CoV-2 infection in golden Syrian hamsters, which showed acute respiratory infection by SARS-CoV-2 infection and are commonly used as an animal model of COVID-19.

We investigated general histopathologic changes induced by SARS-CoV-2 infection at different time points up to 21 days postinfection (dpi). Hamsters were intranasally inoculated with 10 to 10^5 50% tissue culture infectious dose (TCID₅₀) of SARS-CoV-2 or mock control (Table S1). All hamsters infected with SARS-CoV-2 survived with transient weight loss as the primary clinical symptom throughout the study period (Figure 1A). Virus was detected in the lungs at 3 and 5 dpi, followed by viral clearance by 10 dpi (Figure 1B). These results confirmed that SARS-CoV-2 caused acute respiratory infection in hamsters, which is consistent with human cases as previously reported,¹² and that only 10 TCID₅₀ of SARS-CoV-2 is enough to cause disease in hamsters. Seroconversion of SARS-CoV-2 infected hamsters at 21 dpi supported that SARS-CoV-2 replicated well in hamsters regardless of virus dose (Figure 1C). We then analyzed coronal nose sections collected at 3, 5, 10, and 21 dpi (Figure 2A). We observed prominent nasal discharge from the OE as early as 3 dpi (Figure 2B). At 5 dpi, the discharge started to clear, and at 10 and 21 dpi the nasal cavity appeared normal (Figure 2B). To study cellular profiles after SARS-CoV-2 infection, we measured OE thickness in four areas, the nasal septum (S, zone 3), middle- (MT, zone 2), dorsal- (DT, zone 1), and lateral- (LT, zone 4) turbinates (Figure 2A, Figure S1). OEs of infected animals were severely damaged in all areas at 3 dpi and gradually recovered at 5 and 10 dpi, consistent with the previous report.¹³ The OE thickness in S and MT recovered significantly by 21 dpi comparable to the thickness of mock controls (Figure 2B, 2C). The OE at the MT is less damaged than the other areas at 3 dpi, suggesting that the OE of the MT was less vulnerable compared to S, DT, and LT (Figure 2C). Interestingly, the OE turnover rate was different depending on the region. The OE at the S had a faster regeneration than the other regions (Figure 2D). The OE damage induced by SARS-CoV-2 infection was independent of the inoculation dose of SARS-CoV-2 (Figure S2). Together with observed weight loss and seroconversion in hamsters inoculated with even the lowest dose (10 TCID₅₀), SARS-CoV-2 infection seemed to cause OE damage independent of the exposed dose. These findings are consistent with the high rate of human anosmia cases in COVID-19 patients, which is independent of disease severity. We also investigated the presence of SARS-CoV-2

antigens in the OE at different time points postinfection using immunohistochemistry (Figure 3). SARS-CoV-2 antigens were detected in a large proportion of the OE and desquamated epithelial cells at 3 dpi but were undetectable at 5, 10, and 21 dpi (Figure 3B).

To better understand anosmia instigated by SARS-CoV-2 infection, we investigated OE profiles based on zones, as each zone has different characteristics. Recent reports indicate that SARS-CoV-2 infection leads to OE desquamation,¹³ which is the most likely reason for anosmia observed in COVID-19 patients. However, whether the desquamated OE makes a full recovery is unknown. In this study, we show that (1) the OE in the medial areas within the nasal cavity, S and MT, regained full thickness by 21 dpi, and (2) each zone has different susceptibilities and regeneration capabilities after SARS-CoV-2 infection. The reason for this difference associated with zones may be explained by two mechanisms: the influence of air flow¹⁴ within the nasal cavity and/or the blood flow within the nasal tissue. We hypothesize that the medial region of the nasal cavity can clear the virus more effectively compared to the lateral regions based on a wider cavity and more effective air flow, thus limiting exposure time for initial infection due to rapid virus clearance by flushing out. On the other hand, blood flow is generally rich in the nasal septum, which is advantageous for fast tissue recovery. Clinically, as late sequelae of COVID-19, some patients who have recovered from acute COVID-19 maintain persistent symptoms such as depression, anxiety, cognitive impairment, and olfactory dysfunction,¹⁵ and 10–25% of patients after recovering from COVID-19 still suffer from anosmia.¹⁶ A comprehensive psychophysiological smell test indicated the presence of not only peripheral but also central olfactory dysfunction in these patients.^{6,17} However, SARS-CoV-2 antigen was not detected in brain samples from autopsies and viral antigen was barely detectable in cerebrospinal fluid, suggesting that psychiatric and/or neurological sequelae may result from a secondary insult after initial infection.¹⁸ The results of this study may also provide the base knowledge needed for better understanding the mechanisms of late sequelae. CNS symptoms may arise through two mechanisms: deprivation of olfactory inputs or the direct anterograde invasion of the virus into the CNS. For example, 14 days of sensory deprivation in mice has been shown to decrease neurogenesis of granule cells in the olfactory bulb, resulting in altered experience-dependent olfactory memory.^{19–21} Thus, the prolonged damage observed in our study of the OE in the DT (zone 1) and LT (zone 4) may lead

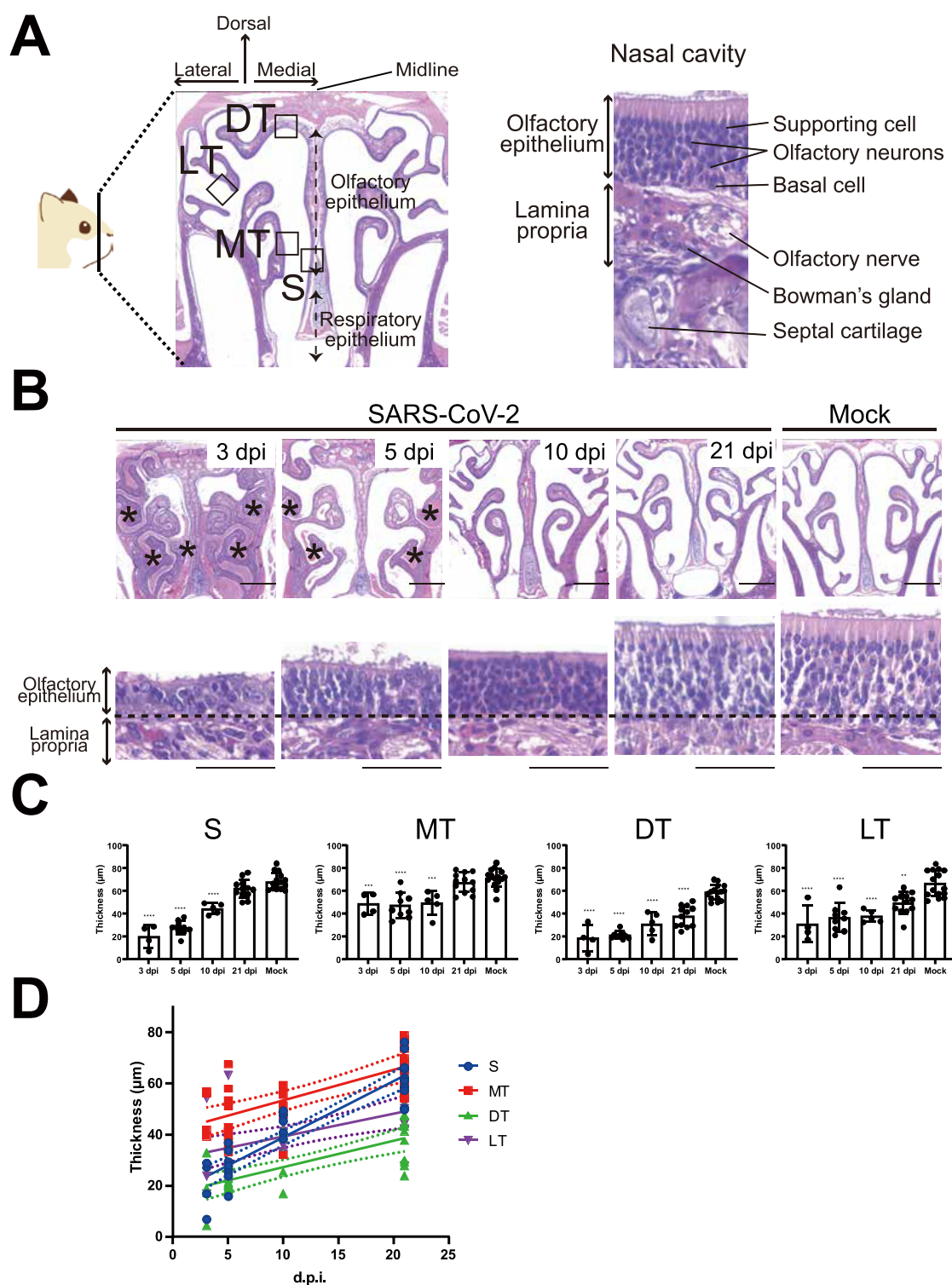


Figure 2. Regeneration of olfactory epithelium after SARS-CoV-2 infection. (A) Representative hematoxylin and eosin (H&E) staining image of the golden Syrian hamster nose. Coronal sections of the snout anterior to the eyes were used to evaluate profiles of the olfactory epithelium (left panel). The OE consists of supporting cells, olfactory sensory neurons, and basal cells (right panel). OE; olfactory epithelium, S; nasal septum, MT; medial turbinate, DT; dorsal turbinate, LT; lateral turbinate. (B) H&E staining of the golden Syrian hamster nose after SARS-CoV-2 or mock infection in low (upper panels) or high (lower panels) magnification. The asterisks represent nasal discharge in the nasal cavity. The border between the OE and lamina propria is indicated by a dashed line. The scale bar represents 1 mm (upper panels) and 50 μm (lower panels). (C) OE thickness in each region (mean \pm SEM). (3 dpi, $n = 4$; 5 dpi, $n = 9$; 10 dpi, $n = 5$; 21 dpi, $n = 12$, Mock, $n = 15$). Statistical analysis was performed with one-way ANOVA followed by Dunnett's multiple comparison test to compare mock groups. ****: $p < 0.0001$, ***: $p < 0.001$, **: $p < 0.01$. (D) Linear regression analysis indicates that the S region features a higher rate of OE proliferation of OE than other regions.

to neurological sequelae altering cognition or impairing memory. The regeneration cycle of OE is precisely regulated

and maintained at 28–35 days regardless of etiology of damage.^{10,11} If the OE is completely restored within this

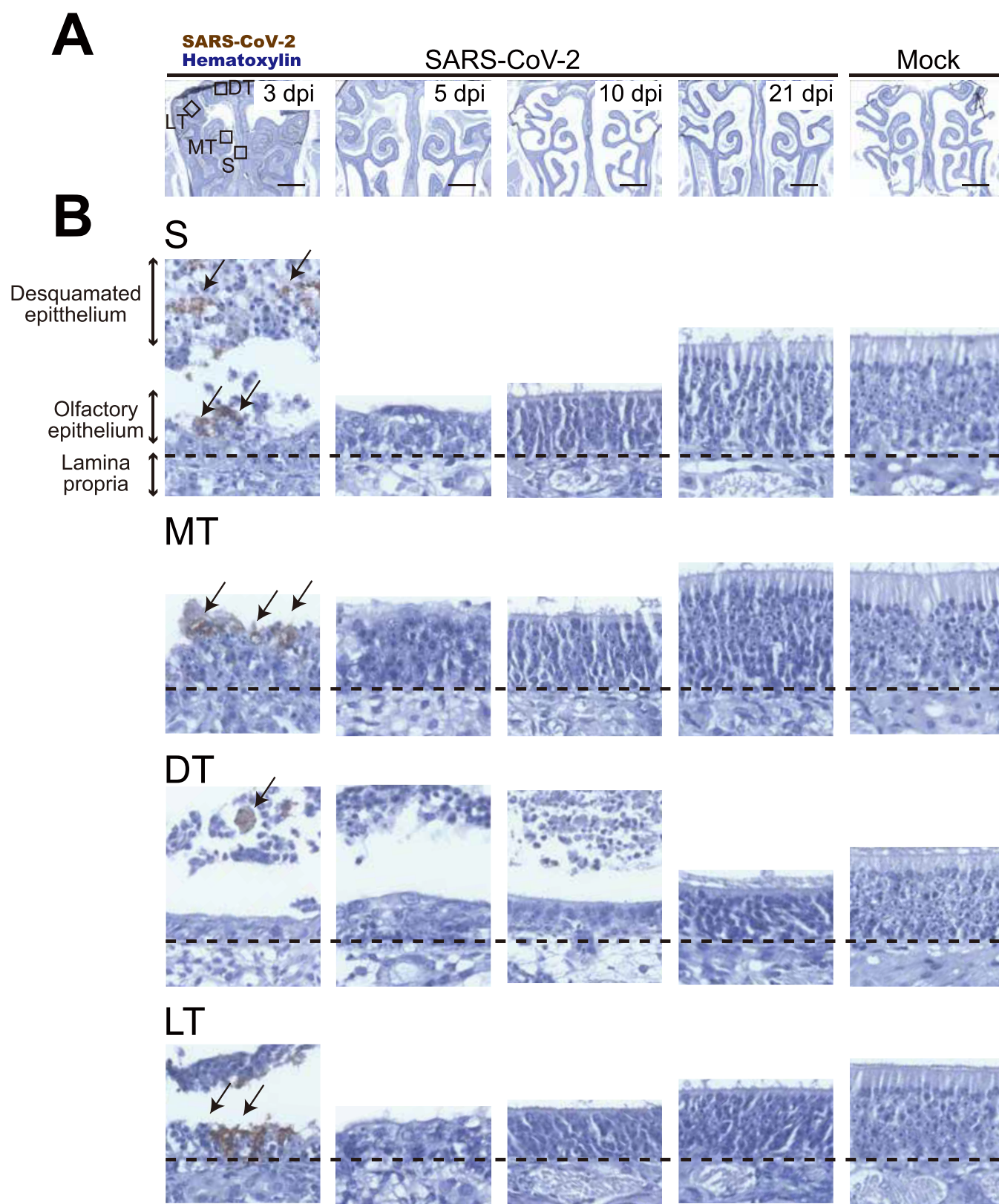


Figure 3. Distribution of SARS-CoV-2 in hamster nose. SARS-CoV-2 antigens in the thin sections were labeled with anti-SARS-CoV-2 nucleocapsid antibody and counter-stained with hematoxylin. Representation of (A) low and (B) high magnification images in the septal area (S). SARS-CoV-2-positive cells are indicated with arrows. Scale bar represents (A) 1 mm or (B) 50 μ m.

critical period, the risk of late sequelae is reduced.^{10,11,22–24} Zonal organization is defined based on the specific ORs, but details on each specific OR and its corresponding odors have

not been fully determined.²⁵ Decreased response to odors of mint and coconut oil was found in patients suffering anosmia due to COVID-19,²⁶ suggesting that receptors for these

odorant molecules may be expressed in slower recovering areas of zone 1 (DT) and zone 4 (LT).

Unfortunately, studies examining olfactory function upon infection with SARS-CoV-2 are limited in terms of animal models. Because zonal organization for hamster nasal cavities has yet to be determined, we roughly correlated the functional zones to the four nasal turbinate areas (S, MT, DT, and LT) based on studies in mice.⁹ Therefore, immunohistochemistry with marker proteins will be necessary to confirm our zonal assignment. Unlike with mice, there are limitations in the availability of immunohistochemical tools for hamsters. Future studies will be performed to further elucidate the mechanisms of SARS-CoV-2-mediated anosmia by utilizing immunolabeling to determine the zonal organization, vulnerability, and regeneration capability of the various nasal zones as well as olfactory behavioral studies, allowing for the correlation of anosmia with damage to specific zones.

METHODS

Cell and Virus. Vero E6 cells were maintained with Dulbecco's modified Eagle's medium (DMEM) supplemented with 10% fetal bovine serum (FBS), 1% penicillin–streptomycin, and L-glutamine. SARS-CoV-2 (USA/WA-1/2020) was propagated in Vero E6 cells with DMEM supplemented with 2% FBS, and cell culture supernatant was stored in the -80°C freezer until use.

Animal Experiments. Six-week-old female hamsters were purchased from Charles River. Hamsters were inoculated with 50–100 μL of SARS-CoV-2 diluted with phosphate-buffered saline or vehicle control intranasally (Figure 1A). Body temperature measurements were performed using subcutaneously implanted BMDS IPTT-300 transponders and the DAS-8007 transponder reader (Bio Medic Data Systems). Body weights were measured using an Ohaus CX1201 Portable Scale. All animals were housed in animal biosafety level-2 (ABSL-2) and ABSL-3 facilities in the Galveston National Laboratory at the University of Texas Medical Branch (UTMB). All animal studies were reviewed and approved by the Institutional Animal Care and Use Committee at UTMB and were conducted according to the National Institutes of Health guidelines.

Virus Titration. Collected lung samples were homogenized with DMEM+2%FBS to make a 10% homogenate. 10-fold serially diluted homogenate samples were inoculated into Vero E6 cells in 96-well plates. After incubation for 72 h at 37°C in a CO_2 incubator, cells were fixed with 10% formalin and stained with 0.25% crystal violet to check for cytopathic effect (CPE). Median tissue culture infectious dose (TCID_{50}) values were calculated by the method of Reed and Muench.²⁷

Neutralization Assay. Serum samples were serially diluted 2-fold with DMEM + 2% FBS and mixed with equal volumes of SARS-CoV-2 diluted to yield 100 $\text{TCID}_{50}/200\ \mu\text{L}$. After incubation for 30 min at 37°C , 100 μL of the virus/serum mixture was inoculated into Vero E6 cells in 96-well plates. Inoculated cells were fixed and stained to check for CPE after 72 h postinoculation as described previously. Neutralization titers were calculated as serum dilution factors with which CPE was completely prevented.

Histological Analysis. Hamsters were euthanized at the end of the study, and the heads of the hamsters were fixed in 10% buffered formalin for 7 days before removal from the BSL-3 facility. Olfactory bulbs and nasal tissue including the olfactory epithelium (OE) were extracted from the skull and decalcified with Kalkitox (Wako, Japan) for 3 h at room temperature with gentle shaking. The decalcified samples were dehydrated in 100% ethanol 3 times and embedded in paraffin. Serial coronal sections of 5 μm thickness were mounted on glass slides. Hematoxylin and Eosin staining was performed after the deparaffinization and rehydration process. To analyze the OE, coronal sections of the OE were divided into four areas along zonal organization (Figure S1). The OE thickness was measured as the distance from the lamina propria to the surface per 100 μm length of OE in each area according to previous reports.¹¹

Immunohistochemistry. To identify SARS-CoV-2 in fixed tissue samples, SARS Nucleocapsid Protein Antibody (Rabbit polyclonal, Novus Biologicals) was used. Deparaffinized sections were autoclaved for 15 min in Target Retrieval Solution (S1700; Dako) for antigen retrieval. Endogenous peroxidases were blocked using 3% hydrogen peroxidase in methanol for 30 min, and nonspecific antibody binding was blocked using Serum-free protein block (X0909; Dako). Samples were incubated at 4°C for 12 h in a solution containing the primary antibodies, followed by a 10 min wash with PBS. The secondary biotinylated antibody (Vectastain Universal Elite ABC PLUS kit, PK-8200; Vector Laboratories) was incubated in avidin–biotin-peroxidase complex (Vectastain Universal Elite ABC PLUS kit, PK-8200; Vector Laboratories). The peroxidase reaction was performed using diaminobenzidine (DAB, ImmPACT DAB, SK-4105; Vector Laboratories).

Statistical Analysis. Statistical analysis was performed using a one-way ANOVA followed by Tukey's post hoc test. $p < 0.05$ was set as statistically significant.

ASSOCIATED CONTENT

Supporting Information

The Supporting Information is available free of charge at <https://pubs.acs.org/doi/10.1021/acschemneuro.0c00649>.

Details on anatomical areas in the olfactory epithelium (Figure S1), changes in thickness of olfactory epithelium in different areas (Figure S2), and animals used in the study (Table S1) (PDF)

AUTHOR INFORMATION

Corresponding Authors

Tomoko Makishima – Department of Otolaryngology, University of Texas Medical Branch, Galveston, Texas 77555, United States; orcid.org/0000-0003-3397-6395; Phone: +1-409-772-9946; Email: tomakish@utmb.edu; Fax: +1-409-772-1715

Slobodan Paessler – Department of Pathology, University of Texas Medical Branch, Galveston, Texas 77555, United States; Phone: +1-409-747-2464; Email: slpaessl@utmb.edu; Fax: +1-409-747-0762

Authors

Shinji Urata – Department of Otolaryngology, University of Texas Medical Branch, Galveston, Texas 77555, United States; Department of Otolaryngology, Graduate School of Medicine, The University of Tokyo, Tokyo 113-0033, Japan

Junki Maruyama – Department of Pathology, University of Texas Medical Branch, Galveston, Texas 77555, United States

Megumi Kishimoto-Urata – Department of Pathology, University of Texas Medical Branch, Galveston, Texas 77555, United States; Department of Otolaryngology, Graduate School of Medicine, The University of Tokyo, Tokyo 113-0033, Japan

Rachel A. Sattler – Department of Pathology, University of Texas Medical Branch, Galveston, Texas 77555, United States

Rebecca Cook – Department of Otolaryngology, University of Texas Medical Branch, Galveston, Texas 77555, United States

Nantian Lin – Department of Otolaryngology, University of Texas Medical Branch, Galveston, Texas 77555, United States

Tatsuya Yamasoba – Department of Otolaryngology,
Graduate School of Medicine, The University of Tokyo,
Tokyo 113-0033, Japan

Complete contact information is available at:
<https://pubs.acs.org/10.1021/acscchemneuro.0c00649>

Author Contributions

[†]S.U. and J.M. contributed equally to this work. S.U. and M.K.U. conceptualized the studies. S.U., J.M., M.K.U., and R.A.S. conducted the experiments. M.K.U. and T.Y. gave technical support and conceptual advice. J.M. and S.P. designed the studies. S.U. analyzed data and wrote the first draft of the manuscript. S.U., M.K.U., T.Y., and T.M. interpreted the results. J.M., R.A.S., R.C., L.N., T.Y., S.P., and T.M. made revisions and edited the manuscript.

Notes

The authors declare no competing financial interest.

ACKNOWLEDGMENTS

We thank K. Kondo, R. Kagoya, C.A. Grant, and M.A. Micci for technical support in preparation of the manuscript. This project was funded by the Clinical and Translational Science Award NRSA (TL1) Training Core (TL1R001440) from the National Center for Advancing Translational Sciences at the National Institutes for Health, National Institute of Allergy and Infectious Disease, National Institutes of Health Award R01 AI129198 and the John S. Dunn Endowment Foundation.

REFERENCES

- (1) Ksiazek, T. G., Erdman, D., Goldsmith, C. S., Zaki, S. R., Peret, T., Emery, S., Tong, S., Urbani, C., Comer, J. A., Lim, W., et al. (2003) A Novel Coronavirus Associated with Severe Acute Respiratory Syndrome. *N. Engl. J. Med.* 348 (20), 1953–1966.
- (2) Luke, T., Wu, H., Zhao, J., Channappanavar, R., Coleman, C. M., Jiao, J. A., Matsushita, H., Liu, Y., Postnikova, E. N., Ork, B. L., et al. (2016) Human Polyclonal Immunoglobulin G from Transchromosomal Bovines Inhibits MERS-CoV in Vivo. *Sci. Transl. Med.* 8 (326), 326ra21.
- (3) Wölfel, R., Corman, V. M., Guggemos, W., Seilmaier, M., Zange, S., Müller, M. A., Niemeyer, D., Jones, T. C., Vollmar, P., Rothe, C., et al. (2020) Virological Assessment of Hospitalized Patients with COVID-2019. *Nature* 581, 465–469.
- (4) Butowt, R., Bilinska, K., and Von Bartheld, C. S. (2020) Chemosensory Dysfunction in COVID-19: Integration of Genetic and Epidemiological Data Points to D614G Spike Protein Variant as a Contributing Factor. *ACS Chem. Neurosci.* 11 (20), 3180–3184.
- (5) Giacomelli, A., Pezzati, L., Conti, F., Bernacchia, D., Siano, M., Oreni, L., Rusconi, S., Gervasoni, C., Ridolfo, A. L., Rizzardini, G., et al. (2020) Self-Reported Olfactory and Taste Disorders in SARS-CoV-2 Patients: A Cross-Sectional Study. *Clin. Infect. Dis.* 71, 1–2.
- (6) Otte, M. S., Klusmann, J. P., and Luers, J. C. (2020) Persisting Olfactory Dysfunction in Patients after Recovering from COVID-19. *J. Infect.* 81 (3), e58.
- (7) Brann, D. H., Tsukahara, T., Weinreb, C., Lipovsek, M., Van den Berge, K., Gong, B., Chance, R., Macaulay, I. C., Chou, H.-J., Fletcher, R. B., et al. (2020) Non-Neuronal Expression of SARS-CoV-2 Entry Genes in the Olfactory System Suggests Mechanisms Underlying COVID-19-Associated Anosmia. *Sci. Adv.* 5801, eabc5801.
- (8) Ueha, R., Kondo, K., Kagoya, R., Shichino, S., Ueha, S., and Yamasoba, T. (2020) ACE2, TMPRSS2, and Furin Expression in the Nose and Olfactory Bulb in Mice and Humans. *Rhinology* 0, 0.
- (9) Yoshihara, Y., Kawasaki, M., Tamada, A., Fujita, H., Hayashi, H., Kagamiyama, H., and Mori, K. (1997) OCAM: A New Member of the Neural Cell Adhesion Molecule Family Related to Zone-to-Zone

Projection of Olfactory and Vomeronasal Axons. *J. Neurosci.* 17 (15), 5830–5842.

(10) Kanaya, K., Kondo, K., Suzukawa, K., Sakamoto, T., Kikuta, S., Okada, K., and Yamasoba, T. (2014) Innate Immune Responses and Neuroepithelial Degeneration and Regeneration in the Mouse Olfactory Mucosa Induced by Intranasal Administration of Poly(I:C). *Cell Tissue Res.* 357 (1), 279–299.

(11) Kikuta, S., Sakamoto, T., Nagayama, S., Kanaya, K., Kinoshita, M., Kondo, K., Tsunoda, K., Mori, K., and Yamasoba, T. (2015) Sensory Deprivation Disrupts Homeostatic Regeneration of Newly Generated Olfactory Sensory Neurons after Injury in Adult Mice. *J. Neurosci.* 35 (6), 2657–2673.

(12) Imai, M., Iwatsuki-Horimoto, K., Hatta, M., Loeber, S., Halfmann, P. J., Nakajima, N., Watanabe, T., Ujie, M., Takahashi, K., Ito, M., et al. (2020) Syrian Hamsters as a Small Animal Model for SARS-CoV-2 Infection and Countermeasure Development. *Proc. Natl. Acad. Sci. U. S. A.* 117 (28), 16587–16595.

(13) Bryche, B., St. Albin, A., Murri, S., Lacôte, S., Pulido, C., Ar Gouilh, M., Lesellier, S., Servat, A., Wasniewski, M., Picard-Meyer, E., et al. (2020) Massive Transient Damage of the Olfactory Epithelium Associated with Infection of Sustentacular Cells by SARS-CoV-2 in Golden Syrian Hamsters. *Brain, Behav., Immun.* 89 (20), 31358.

(14) Kimbell, J. S., Godo, M. N., Gross, E. A., Joyner, D. R., Richardson, R. B., and Morgan, K. T. (1997) Computer Simulation of Inspiratory Airflow in All Regions of the F344 Rat Nasal Passages. *Toxicol. Appl. Pharmacol.* 145 (2), 388–398.

(15) Banda, J. M., Singh, G. V., Alser, O., and PRIETO-ALHAMBRA, D. (2020) Long-Term Patient-Reported Symptoms of COVID-19: An Analysis of Social Media Data. *medRxiv*, DOI: 10.1101/2020.07.29.20164418.

(16) Paderno, A., Mattavelli, D., Rampinelli, V., Grammatica, A., Raffetti, E., Tomasoni, M., Gualtieri, T., Taboni, S., Zorzi, S., Del Bon, F., et al. (2020) Olfactory and Gustatory Outcomes in COVID-19: A Prospective Evaluation in Nonhospitalized Subjects. *Otolaryngol.-Head Neck Surg.* 163, 1–6.

(17) Chen, X., Laurent, S., Onur, O. A., Kleineberg, N. N., Fink, G. R., Schweitzer, F., and Warnke, C. (2020) A Systematic Review of Neurological Symptoms and Complications of COVID-19. *J. Neurol.* 0123456789.

(18) Solomon, I. H., Normandin, E., Bhattacharyya, S., Mukerji, S. S., Keller, K., Ali, A. S., Adams, G., Hornick, J. L., Padera, R. F., and Sabeti, P. (2020) Neuropathological Features of Covid-19. *N. Engl. J. Med.* 383 (10), 989–992.

(19) Petreanu, L., and Alvarez-Buylla, A. (2002) Maturation and Death of Adult-Born Olfactory Bulb Granule Neurons: Role of Olfaction. *J. Neurosci.* 22 (14), 6106–6113.

(20) Yamaguchi, M., and Mori, K. (2005) Critical Period for Sensory Experience-Dependent Survival of Newly Generated Granule Cells in the Adult Mouse Olfactory Bulb. *Proc. Natl. Acad. Sci. U. S. A.* 102 (27), 9697–9702.

(21) Imayoshi, I., Sakamoto, M., Ohtsuka, T., Takao, K., Miyakawa, T., Yamaguchi, M., Mori, K., Ikeda, T., Itohara, S., and Kageyama, R. (2008) Roles of Continuous Neurogenesis in the Structural and Functional Integrity of the Adult Forebrain. *Nat. Neurosci.* 11 (10), 1153–1161.

(22) Ueha, R., Shichino, S., Ueha, S., Kondo, K., Kikuta, S., Nishijima, H., Matsushima, K., and Yamasoba, T. (2018) Reduction of Proliferating Olfactory Cells and Low Expression of Extracellular Matrix Genes Are Hallmarks of the Aged Olfactory Mucosa. *Front. Aging Neurosci.* 10 (MAR), 1–13.

(23) Murai, A., Iwata, R., Fujimoto, S., Aihara, S., Tsuboi, A., Muroyama, Y., Saito, T., Nishizaki, K., and Imai, T. (2016) Distorted Coarse Axon Targeting and Reduced Dendrite Connectivity Underlie Dysosmia after Olfactory Axon Injury. *eNeuro* 3 (5), 0242–16.

(24) Samanen, D. W., and Forbes, W. B. (1984) Replication and Differentiation of Olfactory Receptor Neurons Following Axotomy in the Adult Hamster: A Morphometric Analysis of Postnatal Neurogenesis. *J. Comp. Neurol.* 225 (2), 201–211.

(25) Gaby, J. M., Bakke, A. J., Baker, A. N., Hopfer, H., and Hayes, J. E. (2020) Individual Differences in Thresholds and Consumer Preferences for Rotundone Added to Red Wine. *Nutrients* 12 (9), 2522.

(26) Khare, P., Chander, A. M., Agrawal, K., Singh Jayant, S., Mukherjee, S., Yadav, K., Gupta, R., Chaudhary, S., Srivastava, S., Muralidharan, S., et al. (2020) Utility of Olfactory Test as Screening Tool for COVID-19: A Pilot Study. *medRxiv*, DOI: [10.1101/2020.09.03.20187294](https://doi.org/10.1101/2020.09.03.20187294).

(27) Reed, L. J., and Muench, H. (1938) A Simple method of estimating fifty percent endpoints¹². *Am. J. Epidemiol.* 27 (3), 493–497.